

KC-180-2 Exerts Anti-SCLC Effects via Dual Inhibition of Tubulin Polymerization and Src Signaling

Jian Peng,[§] Yisheng Zeng,[§] Xiaojun Hu,[§] Sheng Huang, Xiaofang Gao, Dong Tian, Shuting Tian, Lan Qiu, Jin Liu, Renhan Dong, Wei Zhan, Chuanjun Qin, Bing Guang,* and Tai Yang*



Cite This: *ACS Omega* 2022, 7, 32164–32175



Read Online

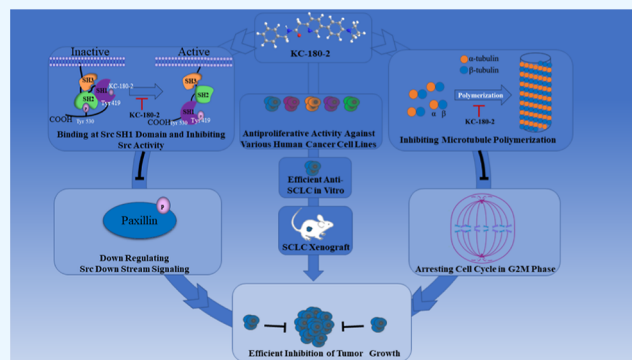
ACCESS |

Metrics & More

Article Recommendations

Supporting Information

ABSTRACT: In this study, a series of *N*-benzyl-2-(5-phenylpyridin-2-yl) acetamide-based derivatives were successfully designed and synthesized as anti-cancer agents. KC-180-2 was screened as a potentially leading compound with dual mechanisms of action: Src signaling and tubulin polymerization inhibition. It efficiently suppressed the proliferation of five cancer cell lines (MDA-MB-231, H446, SKOV-3, HepG2, and HT29), with IC₅₀ values ranging from 5 to 188 nM, especially small-cell lung cancer (SCLC) cells (IC₅₀, 5 nM). Correspondingly, it exerted a significant therapeutic effect on the H446 small-cell lung cancer xenograft model, significantly reducing the volume of tumors without obvious toxicity. Mechanistically, this compound significantly inhibited the polymerization of purified tubulin *in vitro*, inducing G2/M cell cycle arrest and binding to the kinase catalytic domain of the Src protein, which reduced the phosphorylation of Src. Thus, KC-180-2 is a potential lead compound for the further development of a new anti-tumor drug against SCLC.



1. INTRODUCTION

With an estimated 2.2 million new lung cancer cases (11.6% of total cancer cases) and 1.8 million deaths (18.4% of total cancer deaths) worldwide in 2020, lung cancer is the second most commonly diagnosed cancer after breast cancer and remains the leading lethal malignancy.¹ As one of the most lethal lung malignancies, small-cell lung cancer (SCLC) accounts for 15% of all lung cancers and is characterized by an extremely high proliferative rate, strong predilection for early and rapid metastasis, limited therapeutic options, and relatively poor prognosis. The 2-year relative survival rate is 14–15%, and the 5-year relative survival rate is only 7%.²

Treatment mainly depends on the cancer stage, including the limited stage (stages I, II, III, or IV) and extensive stage (stage IV). In a multidisciplinary setting, surgery can be considered the most suitable candidate for patients with stage I SCLC.³ However, less than 5% of people have early-stage SCLC (stage I to stage II) when they are first diagnosed. Radiotherapy with concurrent chemotherapy (etoposide/platinum-based combination chemotherapy) remains the current first-line treatment for both limited- and extensive-stage SCLC worldwide, which has been the case for 2 decades.⁴ Despite the consistent overall response rates of concurrent chemoradiotherapy of $\geq 50\%$,⁵ almost all SCLC patients will inevitably develop drug resistance and tumor recurrence; specifically, 70% of patients with limited-stage SCLC and more than 90% of patients with extensive-stage

SCLC will develop recurrent or progressive disease.⁶ Moreover, the sensitivity of relapsed or progressed SCLC after first-line chemotherapy to further therapies is markedly reduced, and patients who do not receive second-line therapy have a worse prognosis, with a median survival of only 2–3 months.⁷ This statistic suggests an unmet need for the development of chemotherapeutic agents and combinations that exhibit greater anti-tumor effects and superior radiosensitization.

Microtubules are dynamic and ubiquitous cytoskeletal structures that are formed by the self-assembly of α - and β -tubulin heterodimer subunits, playing a key role in cellular functions, such as mitosis and cell division.⁸ Suppressing microtubule dynamics, microtubule inhibitors (MTIs) can be divided into two major groups: microtubule “stabilizers” and “destabilizers”.⁹ The former bind to the tubulin polymer and stabilize microtubules, while the latter bind to the tubulin dimers and destabilize microtubules.¹⁰ Several MTIs have proven to have anti-cancer properties, such as paclitaxel and vincristine, which are so effective against ovarian, mammary, and lung tumors that they have been further investigated in

Received: June 1, 2022

Accepted: August 17, 2022

Published: September 1, 2022



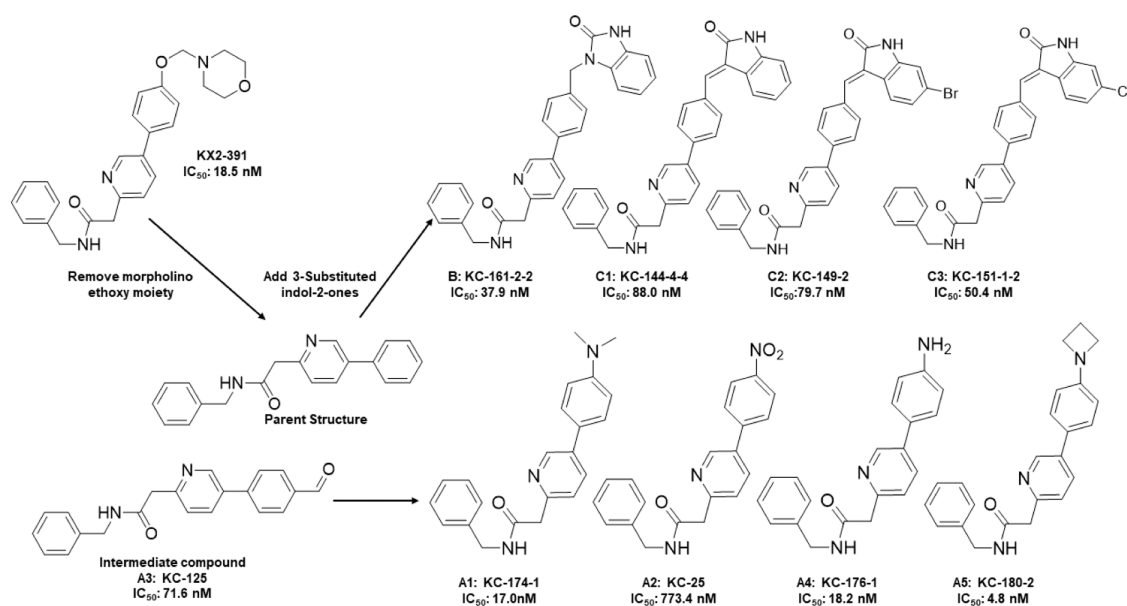


Figure 1. Strategies for the target compound design. The IC_{50} data are derived from the H446 cell line.

Table 1. Effects of Target Compounds against the Cell Viability of Different Cell Lines

Compound	R	$IC_{50} \pm SD^a$ (nM)				
		MDA-MB-231	H446	SKOV-3	HepG2	HT29
KC-144-4-4		109.7±0.1	88.0±0.3	31.8±0.5	125.1±2.2	162.8±0.1
KC-149-2		236.4±0.1	79.7±1.0	74.1±0.2	210.7±0.7	205.7±0.1
KC-151-1-2		147.1±0.1	~ 50.4	34.1±0.7	127.0±1.9	109.9±0.1
KC-161-2-2		286.8±0.2	37.9±0.5	32.6±0.5	124.9±0.3	45.5±0.1
KC-125		527.3±0.1	71.6±0.7	73.1±0.2	146.6±0.2	143.3±0.1
KC-25		2791.0±0.2	733.4±0.4	547.0±0.2	7798.0±0.4	363.7±0.1
KC-174-1		451.4±0.1	~ 17.0	24.3±0.6	32.1±0.2	33.6±0.1
KC-176-1		454.2±0.2	~ 18.2	39.7±0.4	32.9±0.1	46.7±0.1
KC-180-2		187.7±0.1	4.8±1.0	13.9±0.2	14.0±0.1	28.3±0.1
KX2-391		288.8±0.1	18.5±1.4	32.6±0.5	55.4±0.2	61.5±0.1

^aSD, standard deviation. The new compounds at various concentrations were exposed to five cancer cell lines (MDA-MB-231, H446, SKOV-3, HepG2, HT29) for 48 h, and cell viability was detected by CCK-8 ($n = 3$).

clinical trials as potential therapeutic drugs for SCLC or recurrent SCLC since the end of the 20th century.¹¹ However, there has still not been a significant breakthrough in the treatment of SCLC with these MTIs, and they are still essentially ineffective against many other tumors, such as kidney and colon carcinomas and various sarcomas.⁹ Thus, there is still a need to explore new MTIs that could help to improve the therapeutic efficacy.

Src family kinases, including eight non-receptor tyrosine kinases (Src, Fyn, Yes, Lck, Lyn, Hck, Fgr, and Blk), execute pleiotropic functions in regulating adhesion-dependent cell

migration, growth, and survival. Src (c-Src) is a non-receptor tyrosine kinase that is closely correlated with growth factor and cytokine receptors and has vital roles in cell adhesion, angiogenesis, and motility, particularly in the regulation of cancer cell invasion.¹² In addition, the overexpression and high activity of Src are frequently found in lung cancer, including SCLC, especially that of neuroendocrine origin.¹³ In a preclinical immunohistochemical analysis, Src was expressed in 17 of 19 SCLC tumor tissues, while normal lung tissues exhibited low levels of kinase activity,¹⁴ and the Src-kinase inhibitors saracatinib and dasatinib were implemented in a

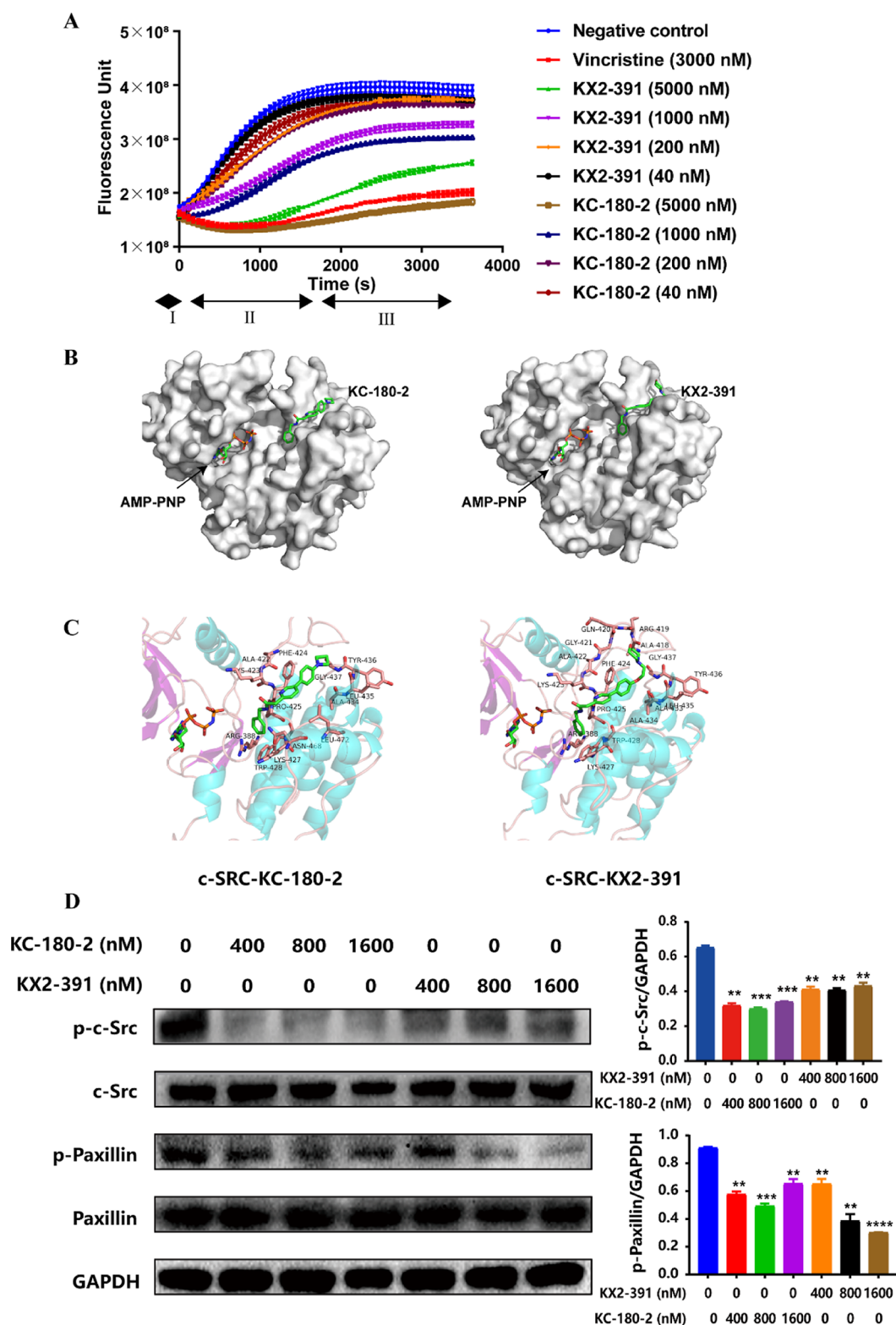


Figure 2. (A) Effects of KC-180-2 on microtubule dynamics in vitro as evaluated by fluorescence density. The signal was measured with excitation at 360 nm and emission at 420 nm. The microtubule polymerization reactions were carried out in the presence of solvent control (DMSO), vincristine (3 μ M), and KX2-391/KC-180-2 (40, 200, 1000, 5000 nM) at 37 $^{\circ}$ C for 1 h. (B) Binding models of KC-180-2/KX2-391 (right, cyan) and a non-hydrolyzable ATP analogue (left binding site) in the Src protein interface pocket (white surface). (C) Interactions between KC-180-2/KX2-391 and associated residues (stick model) in the interface of the homology model for Src (ribbon). (D) Effect of KC-180-2 on Src kinase and Src down-stream signaling. H446 cells were treated with KC-180-2 (200, 400, 800, and 1600 nM) for 8 h. The cell lysates were subjected to immunoblot analysis with antibodies against p-Src, Src, p-paxillin, and paxillin. GAPDH was used as a loading control. Data are expressed as the mean \pm SD of five independent experiments (* P < 0.05, ** P < 0.01, *** P < 0.001, **** P < 0.0001).

phase II trial for patients with SCLC.¹⁵ Thus, Src is a promising therapeutic target for SCLC.

Improving drug activity and circumventing cancer drug resistance by exploiting novel anti-cancer mechanisms are rationales for the ongoing development of novel anti-cancer agents. Additionally, dual inhibitors, in many cases, have been observed to strongly overcome cancer cell resistance compared with their single inhibitor counterparts.¹⁶ For example, Zybrestat, a vascular disrupting agent with a dual mechanism of action as a tubulin-depolymerizing agent and cell junction disrupter, is in phase II/III trials;¹⁷ KX2-391, an *N*-benzyl-substituted acetamide analogue, is a first-in-class dual Src kinase and tubulin polymerization inhibitor being developed as an agent for the treatment of actinic keratosis.^{18,19} KX2-391 has shown activity against various types of cancers, including triple-negative breast cancer, ER-positive breast cancer, and mucinous ovarian cancer, both in vitro and in vivo.²⁰ To improve the anti-solid tumor activity of KX2-391, further lead optimization based on the structure of KX201 was carried out. Derivatives obtained by modifying the morpholine group of KX2-391 exert great activity against colon and ovarian cancer.²¹ Therefore, the present study focused on the discovery of compounds with enhanced anti-cancer activity on the basis of previous research. Accordingly, a series of *N*-benzyl-2-(5-phenylpyridin-2-yl) acetamide-based derivatives were designed, synthesized, and characterized. Among them, KC-180-2 displayed the most promising anti-proliferative activity against various human cancer cell lines, including breast, ovarian, liver, colon, and, especially, SCLC cell lines, with extreme sensitivity. Thus, the present study focused more on SCLC. Our results suggest that KC-180-2 exerts anti-proliferative activity by interfering with both the inhibition of tubulin polymerization and SRC and may be developed as a candidate drug against SCLC.

2. RESULTS AND DISCUSSION

2.1. Chemistry. *N*-Benzyl-2-(5-phenylpyridin-2-yl) acetamide, as the parent structure, was discovered from the first inhibitor (KX2-391, Figure 1) which with dual mechanisms of the Src pathway and tubulin polymerization inhibition was reported in 2018.¹⁸ Smolinski et al. suggested that the side chain of the para position of 3-phenylpyridine and the group of the inter-position of *N*-benzyl were important for influencing the anti-tumor activities. The potency against HT29 was 3-fold enhanced by adding the morpholino ethoxy moiety to the para position of 3-phenylpyridine. However, adding meta-fluorine to *N*-benzyl decreased 5-fold of the potency against HT29. This suggested that altering the morpholino ethoxy moiety may improve the anti-tumor potency.¹⁸ In addition, 3-substituted indolin-2-ones were reported to mediate a variety of biological activities, including tyrosine kinase inhibition, leucine-rich repeat kinase 2 inhibition, and anti-tumor effects, which have been widely applied to compound design strategies for enhancing and expanding the activity of compounds.²² Therefore, KC-144-4-4 was synthesized first and exhibited great anti-tumor activities (Table 1). However, KC-144-4-4 exhibited E/Z isomerism, which was a great challenge for separation of the mixtures of E/Z isomers. To avoid forming the E/Z isomerism, the hydrogen atom on the benzene ring of KC-144-4-4 was replaced by halogen, consequently, producing compounds KC-149-2 and KC-151-1-2. However, the two compounds still retained the characteristics of the E/Z isomerism. Thus, indolin-2-ones were substituted by 2*H*-

benzimidazol-2-one to eliminate the E/Z isomerism by ruling out the double bonds between the parent structure and indolin-2-ones. As a result, KC-161-2-2 was designed, and it also displayed good activities against various tumors, although not surpassing KX2-391 (Table 1). Further, KC-125 is the intermediate product of KC-161-2-2, which also exhibited anti-tumor activities that suggested that some common functional groups, such as amino, *N,N*-dimethyl, and azetidine linked to the parent structure, might display anti-cancer activities and meanwhile avoid the E/Z isomerism. Finally, we found that KC-174-1, KC-176-1, and KC-180-2 displayed remarkable activity in suppressing the proliferation of tumor cells, and KC-180-2 exhibited superior activity to KX2-391, especially to SCLC (Table 1).

2.2. Anti-proliferative Effect of KC-180-2 on Various Cancer Cells and SCLC Cell Lines. The newly synthesized derivatives with similar chemical structures to KX2-391 have potential inhibitory activity against tubulin polymerization. Usually, higher inhibitory activity against cancer proliferation is associated with higher microtubule inhibition. Thus, the compounds were evaluated for their anti-proliferative activities against various human cancer cell lines, including MDA-MB-231 (human breast carcinoma), NCI-H446 (human lung adenocarcinoma), SKOV-3 (ovarian carcinoma), HepG2 (human liver carcinoma), and HT29 (human colorectal carcinoma), and KX2-391 was used as a positive control. IC₅₀ values were obtained from dose–response curves after fitting the data by nonlinear regression. The cytotoxicity of all derivatives on various human cancer cells is summarized in Table 1. Notably, KC-180-2 exhibited the strongest cytotoxic activity in all cell lines compared with the other derivatives. In addition, the SCLC cell line (NCI-H446) was extremely sensitive to KC-180-2 among these cancer cell lines, and the result was subsequently confirmed in another type of adenocarcinoma, SCLC (NCI-H1688 cell line). As shown in Figure 3A, KC-180-2 inhibited cell growth in both SCLC cell lines in a dose-dependent manner. The IC₅₀ value of KC-180-2 toward NCI-H446 cell viability was 5 nM (KX2-391 was 19 nM), and that toward NCI-H1688 was 31 nM (KX2-391 was 34 nM). Thus, KC-180-2 and SCLC were selected for further study.

2.3. Effects of the KC-180-2 Complex on Tubulin Polymerization In Vitro. To assess whether the growth inhibitory effect of these compounds was correlated with an interaction with the tubulin system, we measured their effect on the polymerization of tubulin in a cell-free system, and vincristine was used as a positive control. Under the necessary conditions, tubulin polymerized freely in vitro at 37 °C, and we detected the occurrence of the fluorescence signal during polymerization. The polymerization curve represented three phases of microtubule formation (Figure 2A), namely, nucleation (phase I), growth (phase II), and steady-state equilibrium (phase III). If compounds can bind to tubulin, they often alter one or more characteristic phases of polymerization. Compared with the negative control, vincristine, a microtubule-destabilizing drug, at a final concentration of 3 μM caused a significant decrease in the maximal velocity (V_{max}) of tubulin polymerization and a reduction in the final polymer mass. The inhibition of microtubule polymerization curves induced by KC-180-2 at a final concentration of 5 μM was equivalent to that of vincristine. The fluorescence gradually increased as the concentrations of KC-180-2 and KX2-391 decreased, and they were barely effective in inhibiting

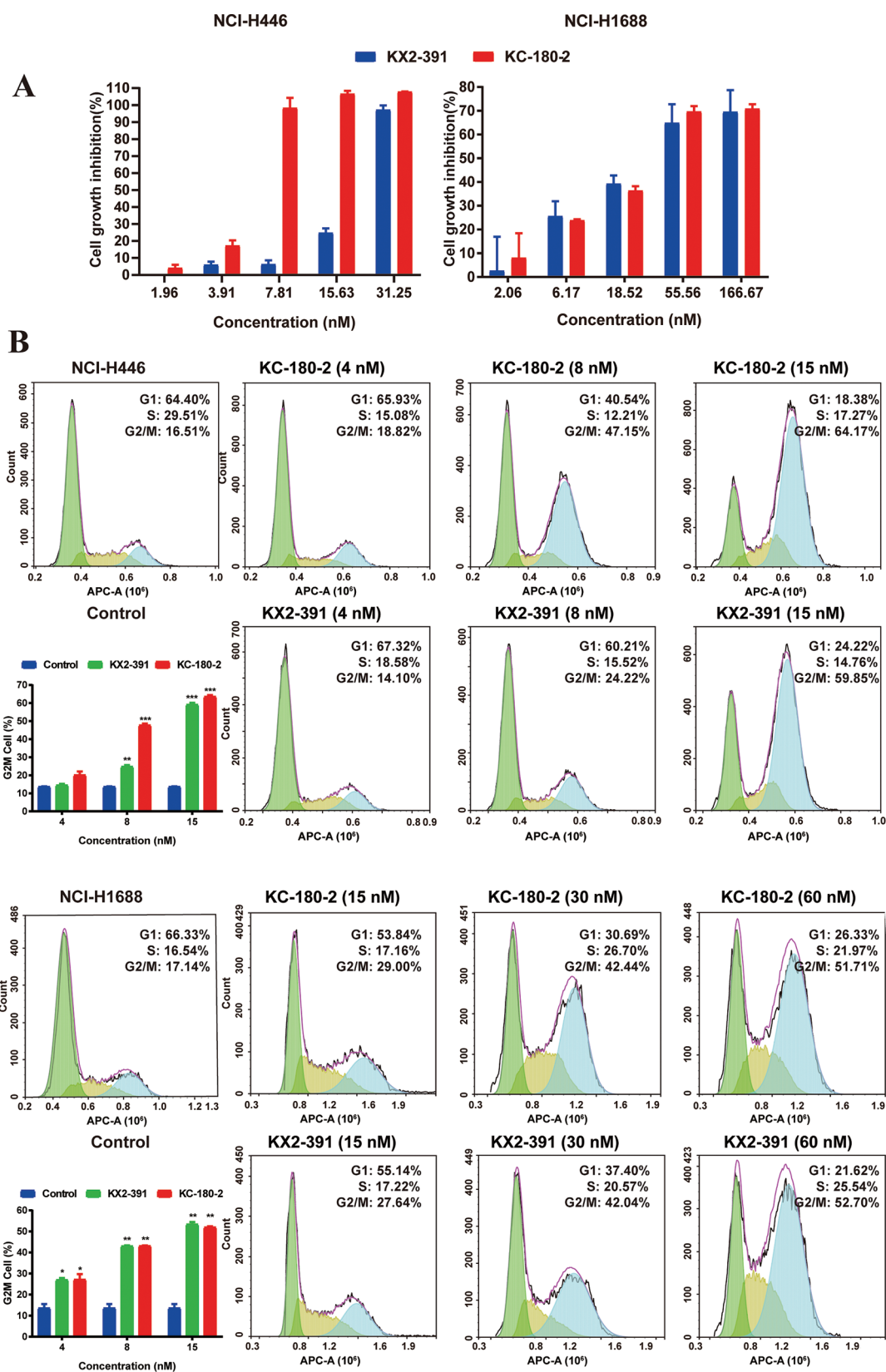


Figure 3. (A) Effect of KC-180-2 on cell viability in the NCI-H446 and NCI-H1688 cell lines. NCI-H446 cells were exposed to KC-180-2 at concentrations of 1.95, 3.90, 7.81, 15.63, and 31.25 nM for 48 h, and NCI-H1688 cells were exposed at concentrations of 2, 6.17, 18.52, 55.56, and 166.67 nM. Control cells were exposed to the solvent only. Cell viability was detected by the CCK-8 assay ($n = 5$). (B) Effects of KC-180-2 on NCI-H446 and NCI-H1688 cell cycle phase arrest. NCI-H446 cells were treated with KC-180-2 at 2, 4, 8, and 15 nM for 24 h, and NCI-H1688 cells were treated at 15, 30, and 60 nM. Then, propidium iodide-stained cells were analyzed by flow cytometry. Data are expressed as the mean \pm SD ($n = 5$, * $P < 0.05$, ** $P < 0.01$, *** $P < 0.001$).

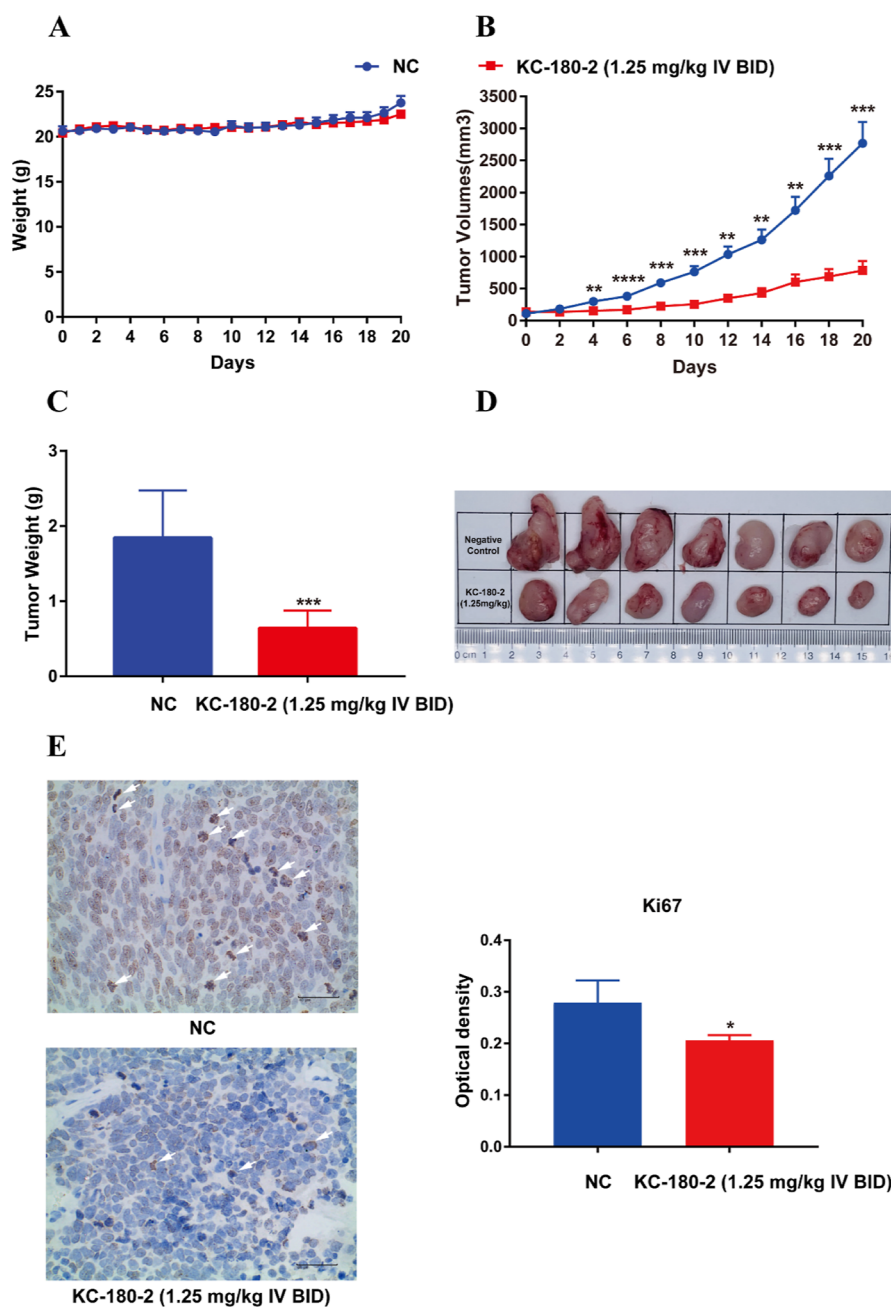


Figure 4. KC-180-2 inhibits the growth of human SCLC xenograft tumors in NOD/SCID mice. NOD/SCID mice were inoculated subcutaneously with 1×10^7 NCI-H446 cells. KC-180-2 (1.25 mg/kg, IV, BID) was dissolved in a solution including 5% DMSO, 15% Kolliphor HS15, and 5% HP- β -CD and administered after the development of an approximate 100 mm³ tumor. Data represent the mean \pm SD ($n = 7$, * $P < 0.05$, ** $P < 0.01$, *** $P < 0.001$). (A) No differences in body weight were observed during treatment. (B) Tumor volume detection. KC-180-2 significantly inhibited tumor growth. (C) Tumor weights of KC-180-2-treated tumors differed significantly from those of the vehicle-treated controls. (D) Tumor images showed that KC-180-2 significantly reduced the tumor size. (E) Tumors were removed from the mice after treatment ended, and immunohistochemical staining for Ki67 assays showed markedly decreased Ki67 in tumors after KC-180-2 treatment ($n = 5$, * $P < 0.05$).

tubulin polymerization at a final concentration of 40 nM. Thus, KC-180-2 inhibited microtubule polymerization by destabilizing microtubules in a dose-dependent manner. Furthermore, KC-180-2 had higher inhibitory activity on microtubule polymerization than KX2-391. In addition, we noted that the tubulin content accounted for approximately 2.5–3.3% of the total protein in cells reported by Hiller and Weber.²³ The final concentration of the purified tubulin we used in the tubulin polymerization assay was 2 mg/mL, which indicated that it was approximately 215- to 284-fold the total tubulin content in $1 \times$

10^6 cells. Therefore, we used 5000 nM KC-180-2 as the final concentration in the tubulin polymerization assay.

2.4. Molecular Docking. In addition to microtubules, Src is another promising molecular target for SCLC therapy. In the present study, molecular docking was performed to elucidate the Src peptide binding mode of complex KC-180-2. The binding mode of complex KC-180-2 in the SH₁ domain of Src is depicted in Figure 2B (KX2-391 as a positive control). The ATP substrate site (left side) was bound with AMP-PNP (a non-hydrolyzable ATP analogue),²⁴ while the right side was

bound with KC-180-2 as a non-ATP competitor. KC-180-2 occupied the same binding pocket as KX2-391, as presented in Figure 2C. This study indicated that KC-180-2 can be well accommodated in a groove, interacting with several hydrophobic residues. In detail, the azetidin-1-yl, acetyl, and *N*-benzyl groups of KC-180-2 interact with Gly437, Pro425, Arg388, and Ans468, respectively, which is slightly different from the positive control, whose morpholinyl, pyridinyl, and *N*-benzyl groups bind with Ala418, Arg419, Pro425, and Arg388, respectively. Notably, residue Arg388 forms salt bridges with phosphates that are essential for maintaining the phosphorylation of Tyr419 in the activation segment of Src.²⁵ KC-180-2 is able to fit to the SH₁ domain of Src protein at the non-ATP substrate site, interacting with Arg388 and consequently breaking the form of activated Src.

2.5. KC-180-2 Downregulated Src Phosphorylation.

The interaction of KC-180-2 against the peptide substrate binding site in Src was investigated through molecular docking, and a cell-based assay further revealed the interaction between KC-180-2 and Src. Therefore, western blotting was performed to measure the levels of the total and phosphorylated proteins after treatment. As expected, KC-180-2 inhibited the phosphorylation of Src (Tyr419), and moreover, it also reduced phosphorylation of paxillin, which is the downstream effector (Figure 2D). Our results demonstrated the downregulation of Src phosphorylation in SCLC cells by KC-180-2 binding to the Src protein at the non-ATP substrate site, which was another significant target by which KC-180-2 exerts its anti-SCLC activity. However, this effect was observed when the KC-180-2 concentration exceeded 400 nM (Figure 2D), whereas cell cycle arrest was evident at concentrations as low as 8 nM (Figure 3A). This result once again indicated that microtubules were the primary target for KC-180-2. Additionally, azetidine substitution for 4-(2-methoxyethyl) morpholine may enhance the ability of KC-180-2 to bind to tubulin while decreasing the affinity to Src.

2.6. KC-180-2 Triggered G2/M Arrest. After NCI-H446 and NCI-H1688 treatment with KC-180-2 for 48 h, the proliferation of both cell lines was significantly inhibited (IC₅₀ = 5 nM), and NCI-H446 cells were more sensitive than NCI-H1688 cells (Figure 3A). Interference microtubule polymerization may induce cell cycle arrest in the G2/M phase and further inhibit cancer cell proliferation. To explore the effect of KC-180-2 on cell cycle progression, we used flow cytometry to analyze the cell cycle distribution of NCI-H446 and NCI-H1688 cells. As shown in Figure 3, KC-180-2 caused remarkable and concentration-dependent G2/M arrest in both cell lines following 24 h of treatment, whereas the control cells were primarily in the G1 and S phases. KC-180-2 induced obvious G2/M arrest at 8 nM in the NCI-H446 cell line, while KX2-391 (positive control) had no obvious effect on G2/M arrest. When cells were exposed to 15 nM KC-180-2 and KX2-391, the percentage of NCI-H446 cells in G2/M increased from 16.51 to 64.17 and 59.85%, respectively. As the negative control, the percentage of NCI-H1688 cells in G2/M was 17.14%; when cells were exposed to 60 nM KC-180-2 and KX2-391, the percentage of G2/M phase cells increased to 51.57 and 52.70%, respectively. Taken together, KC-180-2 strongly induced the accumulation of mitotic cells and arrested cells in the G2/M phase in a concentration-dependent manner (Figure 3B), eventually inhibiting cell proliferation, which was attributed to its ability to prevent microtubule polymerization (Figure 2A) and indicated that KC-180-2 was a microtubule-

destabilizing agent inducing mitotic catastrophe. Interestingly, our study revealed very similar concentration levels of KC-180-2 between the inhibition of cell proliferation and the arrest of the cell cycle, indicating that the inhibition of cancer cell proliferation was mainly achieved by interfering with tubulin polymerization.

2.7. KC-180-2 Inhibited Tumor Xenograft Growth.

Finally, to further validate the anti-tumor efficiency of KC-180-2 in vivo, an NCI-H446 xenograft model was applied. In the present study, the compound was not administered until the volume of the xenograft grew to at least 100 mm³. During the treatment period, the KC-180-2 group did not exhibit an obvious decrease in mouse body weight compared with the negative control group (Figure 4A), indicating that KC-180-2 had no obvious toxicity at a dose of 1.25 mg/kg via intravenous injection (IV) twice a day (BID). The average tumor weight of the mice in the KC-180-2 group was 0.64 ± 0.23 g, while that of the mice in the negative control group was 1.85 ± 0.63 g (Figure 3C). Notably, as shown in Figure 4B,D, along with the tumor weight, KC-180-2 caused a distinct inhibition of tumor growth at that dose compared with the vehicle, with a tumor growth inhibition (TGI %) of 75% at the end of the study. In summary, the results of the present study indicate that KC-180-2 has great potential as an anti-SCLC compound.

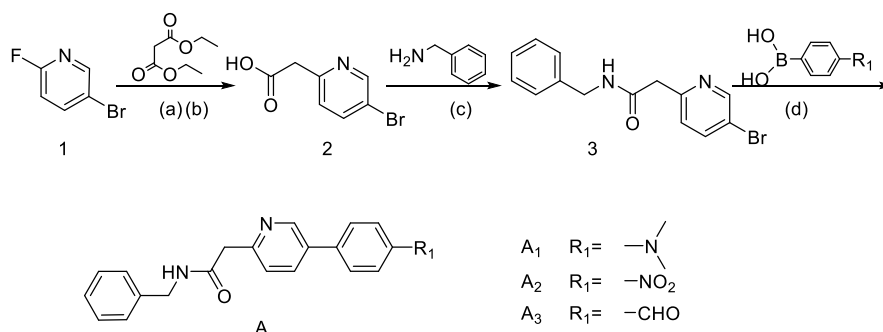
Ki-67 is a nuclear antigen that is expressed in the growth and synthesis phases of the cell cycle but not in the resting phase.²⁶ The present study showed that KC-180-2 can observably inhibit cell proliferation in vitro; thus, Ki67, as a cell proliferation marker, was used to detect proliferating cells in vivo. As shown in Figure 4E, in the KC-180-2 group, the proportion of Ki67-positive cells among the total population of tumor cells was significantly decreased compared with that in the negative control group. The results indicated that after treatment, proliferation decreased significantly in vivo, which was in accordance with the in vitro results. Next, we aimed to identify whether KC-180-2 exerts activity against MTI-resistant cell lines and elucidate the detailed mechanisms of KC-180-2.

3. CONCLUSIONS

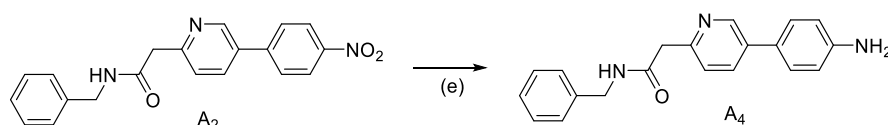
In the present study, we successfully designed and synthesized a series of *N*-benzyl-2-(5-phenylpyridin-2-yl) acetamide-based derivatives and evaluated their anti-proliferative activity in a variety of cancer cell lines. Compound KC-180-2 exhibited significant anti-proliferative activity against SCLC cancer cells with IC₅₀ values of 4.8–31.5 nM. Moreover, we revealed that KC-180-2 exerted its anti-proliferative effect through its dual mechanism of inhibiting Src phosphorylation and tubulin polymerization. KC-180-2 downregulated Src phosphorylation by binding to SH₁ of Src and interfered with microtubule polymerization, causing cell cycle arrest at the G2/M phase and eventually inducing mitotic catastrophic cell death. In addition, further investigation using an NCI-H446 xenograft model revealed remarkably potent anti-tumor activities in vivo, with a TGI (%) of 75% and without any obvious toxic effect at a dose of 1.25 mg/kg (IV, BID). In conclusion, KC-180-2 serves as a potential anti-SCLC lead compound for further development.

4. MATERIALS AND METHODS

4.1. Materials. NCI-H1688, SK-OV-3, MDA-MB-231, HT-29, HepG2, and NCI-H446 cell lines were purchased from the American Type Culture Collection (Rockville, MD,

Scheme 1. Synthetic Methods for the Preparation of A1, A2, and A3^a

^aConditions: (a) malonic diethyl ester, DMSO, Cs₂CO₃, 80 °C, 16–20 h; (b) MeOH, 30% NaOH, 16–20 h, 60 °C; (c) benzylamine, DMF, DIPEA, TBTU, overnight, rt; (d) phenylboronic acid derivative, 1,4-dioxane/H₂O, Pd[P(C₆H₅)₃]₄, K₂CO₃, 80 °C, 10–12 h.

Scheme 2. Synthetic Methods for the Preparation of A4^a

^aConditions: (e) EtOH, Fe, NH₄Cl, 90 °C, 4–8 h.

USA). McCoy's 5A, DMEM, RPMI-1640 medium, and fetal bovine serum (FBS) were purchased from Gibco (Gaithersburg, MD, USA); the absorbance and fluorescence were measured using a Victor Nivo Microplate Reader (Perkin Elmer, German); a Cell Cycle Assay Kit was purchased from US Everbright Inc. (Suzhou, China); a tubulin polymerization assay kit (BK011P) was purchased from Cytoskeleton Inc. (Denver, CO, USA); Western blot analyses were performed with primary antibodies against the following antigens: mouse anti-phospho-c-Src (1:100; Santa Cruz Cat# sc-81521), mouse anti-c-Src (1:200, Santa Cruz Cat# sc-8056), anti-paxillin (pY118) antibody (1:500; Cohesion Biosciences Cat# CPA3307), anti-paxillin (1:500; Santa Cruz Cat# sc-365379), rabbit anti-GAPDH (1:1000; Cell Signaling Technology Cat# 2118), anti-rabbit IgG, HRP-linked antibody (1:4000; Cell Signaling Technology Cat# 7074), anti-mouse IgGκ, and HRP-linked antibody (1:4000; Santa Cruz Cat# sc-516102). Five-week-old female non-obese diabetic (NOD)/severe-combined immunodeficient mouse (SCID) and male Sprague–Dawley rats were obtained from Weitonglihua (Beijing, China).

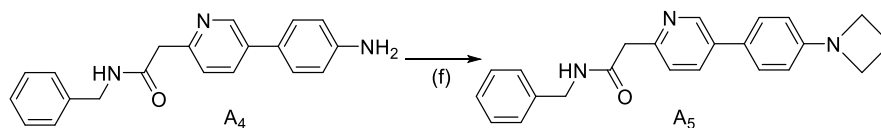
4.2. General Procedure for the Synthesis of A1 (KC-174-1), A2 (KC-25), and A3 (KC-125). 5-Bromo-2-fluoropyridine (1, 0.28 mol) and malonic diethyl ester (0.71 mol) were stirred and dissolved in 1 L of DMSO before adding cesium carbonate (0.71 mol) and reacted for 16–20 h at 80 °C. Thin-layer chromatography (TLC) was used to identify the completion of the reaction. After cooling to room temperature, the reaction solution was diluted in 2 L of distilled water and then extracted three times with 500 mL of ethyl acetate. The ethyl acetate extracts were washed twice with 150 mL of water and concentrated to dryness under reduced pressure.

Methanol (300 mL) and 200 mL of 30% sodium hydroxide were added to the above concentrated products. Then, the solution was stirred for 16–20 h at 60 °C. TLC analyses were used to monitor the reaction process. After the reaction had gone to completion, the solution was concentrated to reduce the volume to approximately 200 mL under reduced pressure.

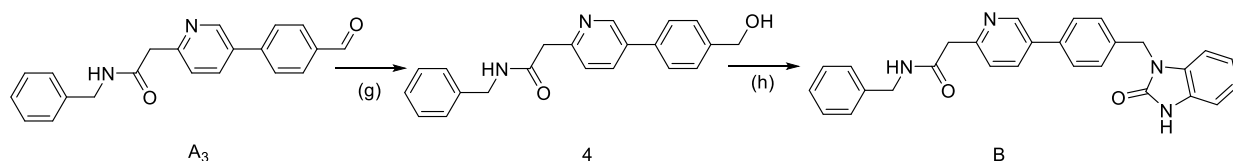
The solution was cooled, and the pH value was adjusted to 4.0–5.0 with 4 M hydrochloric acid and left for approximately 1 h for product precipitation. The solid product was filtered and washed twice with distilled water and once with ethyl acetate. Then, intermediate 2 was obtained by drying.

Intermediate 2 (18.0 g, 83.3 mmol) and benzylamine (17.8 g, 166.6 mmol) were dissolved in 150 mL of *N,N*-dimethylformamide (DMF) and *N,N*-diisopropylethylamine (DIPEA, 166.6 mmol). Then, *O*-(enzotriazole-1-yl)-*N,N,N',N'*-tetramethyluronium tetrafluoroborate (TBTU, 40.1 g, 125.0 mmol) was slowly added to the solution and stirred overnight at room temperature. After the completion of the reaction, 500 mL of ethyl acetate and 1 L of distilled water were added to the solution, and the mixture was allowed to stand for phase separation. Then, the ethyl acetate layer was collected and washed twice with 90 mL of 5% potassium carbonate and twice with 50 mL of a saturated solution of sodium chloride. The sample was collected and dried with 35 g of anhydrous sodium sulfate for 1 h. Then, sodium sulfate was removed by filtration, and the product was concentrated to dryness under reduced pressure. The residue was crystallized by petroleum ether, and intermediate 3 was obtained by filtration.

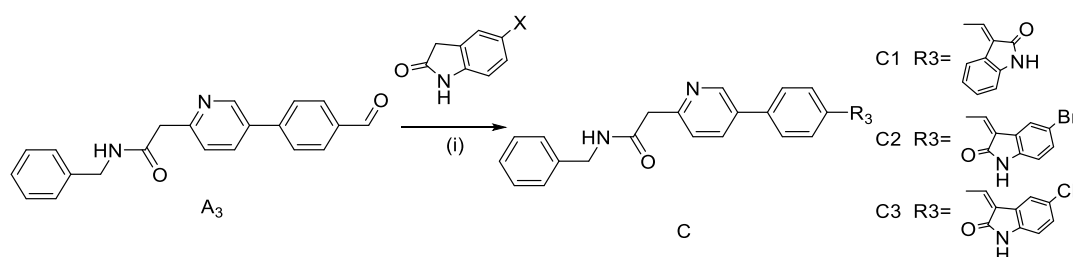
Intermediate 3 and phenylboronic acid derivatives (1:1.5) were dissolved in dioxane, and potassium carbonate solution was added. Then, the catalyst Pd[P(C₆H₅)₃]₄ was added to the above solution, and the reaction was heated to approximately 80 °C for 12 h. After the flask cooled to room temperature, ethyl acetate and water were added to the solution and allowed to stand to achieve phase separation. The aqueous layer was extracted twice with ethyl acetate and combined with the organic extract. The extract was washed three times with 5% sodium hydroxide, followed by 5% dilute hydrochloric acid, and finally washed with saturated sodium chloride solution until neutral. Then, the sample was collected and dried with anhydrous sodium sulfate for 1 h. Sodium sulfate was removed by filtration, and the filtrate was concentrated to dryness under reduced pressure. The residue was crystallized by methyl *tert*-

Scheme 3. Synthetic Methods for the Preparation of A5^a

^aConditions: (f) DMF, 1,3-dibromopropane, K₂CO₃, 60 °C, 12 h.

Scheme 4. Synthetic Methods for the Preparation of B^a

^aConditions: (g) EtOH, NaBH₄, 0 °C, 4 h; (h) PPh₃, THF, DIAD, 2-benzimidazole, overnight, rt.

Scheme 5. Synthetic Methods for the Preparation of C1, C2, and C3^a

^aConditions: (i) 2-indolinone derivative, PhMe, PTSA, refluxing, 12–16 h.

butyl ether, and compounds A1–A3 were obtained by filtration, purity: >95%, yield: 73–80% (Scheme 1).

4.3. General Procedure for the Synthesis of A4 (KC-176-1). Compound A2 (2.00 g, 5.76 mmol) was suspended in 80% ethanol. Then, iron powder (0.97 g, 17.37 mmol) and ammonium chloride (0.92 g, 17.20 mmol) were added to the solution, and the temperature was increased to 90 °C for 4–8 h. The solution was cooled to room temperature and filtered. The filtrate was concentrated and dissolved in 40 mL of ethyl acetate. The organic layer was washed with 40 mL of saturated sodium chloride solution and dried with anhydrous sodium sulfate for 1 h. After removing sodium sulfate by filtration, the residue was concentrated to dryness under reduced pressure. The oily substance was purified by column chromatography (eluent: ethyl 1:3 acetate/petroleum ether) to obtain compound A4, purity: 97%, yield: 90.1% (Scheme 2).

4.4. General Procedure for the Synthesis of A5 (KC-180-2). Compound A4 (1.00 g, 3.15 mmol) was dissolved in 25 mL of DMF, and then 1,3-dibromopropane (0.64 g, 3.17 mmol) and potassium carbonate (0.87 g, 6.29 mmol) were added into the solution, followed by stirring for 12 h at 60 °C. The solution was cooled to room temperature, poured into 100 mL of ice-cold water, and extracted with 75 mL of ethyl acetate three times. The organic layer was collected, washed twice with saturated sodium chloride solution, and dried with anhydrous sodium sulfate (15 g) for 1 h. After removing the sodium sulfate by filtration, the residue was concentrated to dryness under reduced pressure and further purified by column chromatography (eluent: methanol/dichloromethane 1:2) to obtain compound A5, purity: 98.5%, yield: 45% (Scheme 3).

4.5. General Procedure for the Synthesis of B (KC-161-2-2). Compound A3 (2.00 g, 6.05 mmol) was dissolved

in 20 mL of ethanol. After the solution was cooled to 0 °C, sodium borohydride (0.46 g, 12.16 mmol) was added to the solution and allowed to react for 4 h. Eighty milliliters of water was added to the solution and extracted with 100 mL of ethyl acetate. The ethyl acetate layers were collected and washed once with 5% hydrochloric acid, followed by washing with 60 mL of saturated sodium chloride solution until achieving a neutral pH and drying with anhydrous sodium sulfate (5 g) for 30 min. Then, sodium sulfate was removed by filtering, and the filtrate was concentrated to dryness to obtain intermediate 4.

Triphenylphosphine (3.17 g, 12.08 mmol) was dissolved in 15 mL of tetrahydrofuran (THF), which was cooled to 0 °C in an ice bath. Then, diethyl azodicarboxylate (DIAD, 2.45 g, 12.12 mmol) was added to the solution. Next, intermediate 4 and 2-benzimidazolone (0.80 g, 6.05 mmol) were dissolved in 15 mL of THF, which was slowly added to the above solution for reaction overnight at room temperature. After the reaction was completed, the solution was concentrated to dryness under reduced pressure. The residue was further purified by column chromatography (ethyl acetate/petroleum ether 1:1) to obtain compound B, purity: 98.5%, yield: 81% (Scheme 4).

4.6. General Procedure for the Synthesis of C1 (KC-144-4-4), C2 (KC-149-2), and C3 (KC-151-1-2). Compound A3 and a 2-indolinone derivative (an equivalence ratio of 1:1.3) were dissolved in 5 times volume (mL/g) of toluene, and *p*-toluenesulfonic acid (PTSA) was added to catalyze the reaction with refluxing for 12–16 h. After the reaction was completed, the solution was cooled to room temperature. The organic layer was washed with water, followed by saturated sodium chloride solution, and then dried with anhydrous sodium sulfate. After removing sodium sulfate, the organic layer was concentrated to dryness under reduced pressure. The

residue was further purified by column chromatography (ethyl acetate/petroleum ether 1:1) to obtain compounds C1–C3, purity: >98%, yield: 55–70% (Scheme 5).

4.7. Molecular Docking. The 2D structure of the compound was then converted into the corresponding 3D coordinates using the Babel server (<http://openbabel.sf.net>). The Python script “prepare_ligand4.py” was used to convert the ligand to pdbqt format, with the assigned atom type and partial charge. All rotatable bonds in the ligand were set as flexible to perform flexible docking. A homology model of the target protein was built by Modeler 9.23 (Laboratory of Andrej Sali, USA) using the crystal structures of Iir3 and 2src as templates. One hundred independent structures were constructed, and the one with the best DOPE score was chosen for further energy minimization in Amber18 using the ff14SB force field. The relaxed model was saved as a pdb file and converted to pdbqt format as a docking receptor using AutoDockTools-1.5.6 (The Scripps Research Institute, USA), with the assigned atom type and partial charge. The receptor was kept as rigid during docking. Vina1.1.2 (Molecular Graphics Lab at The Scripps Research Institute, USA) was used to perform molecular docking. The docking boxes were set at the peptide binding site of c-Src. The search exhaustiveness was set to 32, and the number of binding modes was set to 9. Other parameters were kept at the default settings.

4.8. Cell Culture. NCI-H1688, SK-OV-3, MDA-MB-231, HT-29, HepG2, and NCI-H446 cells were, respectively, in RPMI-1640, RPMI-1640, RPMI-1640, McCoy's 5A, DMEM, and RPMI-1640 medium supplemented with fetal bovine serum and penicillin (50 U/mL)–streptomycin (100 mg/mL). Cells maintained at 37 °C and 5% CO₂.

4.9. Cell Viability Assay. Cell viability was measured using Cell Counting Kit-8 (CCK-8, 96992 Sigma-Aldrich). Cell suspensions (100 μL, 7000 cells per well) were dispensed in a 96-well plate for 12 h before treatment. Cells were exposed to predetermined and different dilutions (100 μL) of compounds in a humidified incubator (e.g., at 37 °C, 5% CO₂) for 48 h. Ten microliters of CCK-8 solution was added to each well of the plate, which was then incubated for 4 h. A microplate reader (PerkinElmer, USA) was used to measure the absorbance of the sample at 450 nm. The mean optical density (OD, absorbance) of the indicated groups was used to calculate the percentage of cell viability = $[(A_t - A_b)/(A_c - A_b)] \times 100$, where A_t = absorbance value of the test compound, A_b = absorbance value of the blank, and A_c = absorbance value of the control. IC₅₀ values were calculated using GraphPad Prism 7.0 statistical software (GraphPad Software Inc.; San Diego, CA, USA). Values were plotted by averages of triple or quintuple duplicate wells.

4.10. Cell Cycle Analysis. Cell cycle analysis was performed using a Cell Cycle Assay Kit Plus (Biotechnology Co., Ltd, Suzhou, China). Cells were seeded at a density of 6×10^5 cells/well in 24-well plates. Following attachment, NCI-H1688 cells were treated with KC-180-2 and KX-391 at final concentrations of 15, 30, and 60 nM for 24 h, and H446 cells were treated with concentrations of 4, 8, and 15 nM. After incubation, the cells were harvested and resuspended in PBS. After centrifugation at 800g for 5 min, cells were fixed with 70% ice-cold ethanol overnight at 4 °C. After pelleting the cells with centrifugation at 1000g for 7 min, 1 mL of PBS was added to resuspend the cells. Then, 4 μL of Red Nucleus I staining solution was added to each sample, mixed slowly and thoroughly, and incubated in the dark at room temperature

for 20 min. A NovoCyte flow cytometer (ACEA Biosciences, San Diego, USA) and NovoExpress 1.4.0 software (ACEA Biosciences, Inc., San Diego, USA) were used to measure and analyze the DNA cell cycle.

4.11. Effects of KC-180-2 on Tubulin Polymerization In Vitro. In the presence of GTP and Mg²⁺, αβ-tubulin is known to be able to self-assemble (polymerize) in vitro into microtubules at physiological temperature (37 °C). By incorporating a fluorescent reporter into microtubules as tubulin polymerization occurs, assembly can be monitored in vitro.²⁷ A tubulin polymerization assay kit (Cytoskeleton Inc., Denver, CO, USA) was used in this assay to determine the effects of compounds on tubulin polymerization. After incubating the samples for 1 min at 37 °C, KC-180-2, KX-391, or the positive control (vincristine) at various concentrations were mixed with GTP stock (100 mM) at a final concentration of 1 mM and purified neuronal tubulin reaction (10 mg/mL) at a final concentration of 2 mg/mL. After shaking for 5 s, the plate was read immediately with a microplate reader (Ex. 340–360 ± 20 nm, Em. 410–460 ± 20 nm) at 37 °C for 1 h. Values were plotted by averages of quintuple duplicate wells.

4.12. Western Blot Analysis. H446 cells were lysed in RIPA buffer containing protease and phosphatase inhibitor cocktail (Roche Applied Science). Equal amounts of total cellular proteins (40 μg/lane) were separated by SDS-polyacrylamide gel electrophoresis and transferred to polyvinylidene fluoride membranes (Roche Company, Basel, Switzerland). Membranes were blocked in TBS-Tween (TBS-T) with 5% non-fat dry milk for 1 h at 37 °C and probed with specific antibodies at 4 °C overnight. After washing with TBS-T, the membranes were incubated with the secondary antibody for 1 h and visualized using an ECL Western blot detection kit (Millipore, USA).

4.13. Xenograft Experiments. The Ethics Commission of Chengdu Medical College approved the animal studies described herein. NOD/SCID mice ($n = 14$) were housed in sterile exhaust ventilated cages with HEPA-filtered sterile air in the barrier system of the SPF laboratory, and they were housed for 1 week to allow them to adapt to the environment before the experiment started. A total of 1×10^7 NCI-H446 cells in 100 μL of PBS and 100 μL of Matrigel basement membrane matrix (Corning, NY, USA) were subcutaneously injected into the right flank of NOD/SCID mice, and tumor growth was monitored by caliper measurements. When the tumors grew to approximately 100 mm³ in diameter, mice were randomized into a control group and a KC-180-2-treated group (KC-180-2 group, $n = 7$, 1.25 mg kg⁻¹, IV, BID). KC-180-2 was dissolved in a solution including 5% DMSO, 15% polyoxyxyl 15 hydroxystearate (Kolliphor HS15), and 5% hydroxypropyl-β-cyclodextrin (HP-β-CD). The negative control group ($n = 7$) was injected with the above solution. Treatment was continued for up to 20 days from the date of randomization (day 0). The tumor volume was measured with Vernier calipers at 2 day intervals and was calculated using a standard formula: (shortest diameter)² × (longest diameter) × 0.5. When the average tumor volume reached 2000 mm³, mice were killed, according to institutional guidelines. TGI (%) was determined using the formula $TGI (\%) = (V_c - V_t)/(V_c - V_0) \times 100$, where V_c and V_t are the mean tumor volumes of the control and treated groups at the end of the study (day 20), respectively, and V_0 is the tumor volume at the start of the study (day 0). TGI >50% was considered meaningful. After the end of this experiment,

mice were euthanized by intraperitoneal injection of sodium pentobarbital (150 mg/kg).

4.14. Immunohistochemistry. Section 4 μm thick were cut from xenograft tumor tissues that were fixed in 10% neutral buffered formalin and embedded in paraffin after dehydration before being placed on slides, and immunohistochemical analysis for Ki67 (1:20; Abcam; Cat# 16667) was carried out. Antigen retrieval was conducted using microwave oven heating in 0.01 M citrate buffer at a pH of 6.0 after inactivating the endogenous peroxidase using 3% hydrogen peroxide solution. After blocking with normal goat serum, rabbit monoclonal antibody was added to the sections and incubated at 4 °C overnight. Slides were then incubated with biotinylated goat anti-rabbit IgG and streptavidin-HRP (Zhong Shan Golden Bridge Bio, China, Cat# SP-9001) for 30 min. After washing three times with PBS, the immunocomplexes were stained with 3'-diaminobenzidine (DAB, Zhong Shan Golden Bridge Bio, China, Cat# K135925C) at room temperature and then counterstained with Harris' hematoxylin. Image-Pro Plus 6.0 software (Media Cybernetics, Silver Spring, USA) was used to detect the integrated optical density (IOD) and area of all images collected using a microscope.

4.15. Statistical Analysis. Statistical analysis was performed using Prism 7 (GraphPad Software, La Jolla, CA, USA) and SPSS 17.0 software (SPSS, Inc., Chicago, IL, USA). Data are provided as the mean \pm SD or mean \pm SEM unless otherwise indicated. The differences between the means of the control group and treatment group were measured by *t*-tests, and differences with a probability less than 0.05 were considered significant.

■ ASSOCIATED CONTENT

SI Supporting Information

The Supporting Information is available free of charge at <https://pubs.acs.org/doi/10.1021/acsomega.2c03408>.

Additional spectroscopic characterization data of all the synthesized compounds and the IC₅₀ value curves of all compounds against five different cell lines (PDF)

■ AUTHOR INFORMATION

Corresponding Authors

Bing Guang – Chengdu Biobel Biotechnology Co., Ltd., Chengdu, Sichuan Province 610094, China; Email: guangb@yahoo.com

Tai Yang – School of Pharmacy, Chengdu Medical College, Chengdu, Sichuan Province 610500, China; orcid.org/0000-0002-2145-7435; Email: taiyang@cmc.edu.cn

Authors

Jian Peng – School of Pharmacy, Chengdu Medical College, Chengdu, Sichuan Province 610500, China

Yisheng Zeng – School of Pharmacy, Chengdu Medical College, Chengdu, Sichuan Province 610500, China

Xiaojun Hu – School of Pharmacy, Chengdu Medical College, Chengdu, Sichuan Province 610500, China

Sheng Huang – Chengdu Biobel Biotechnology Co., Ltd., Chengdu, Sichuan Province 610094, China

Xiaofang Gao – School of Pharmacy, Chengdu Medical College, Chengdu, Sichuan Province 610500, China

Dong Tian – School of Pharmacy, Chengdu Medical College, Chengdu, Sichuan Province 610500, China

Shuting Tian – School of Pharmacy, Chengdu Medical College, Chengdu, Sichuan Province 610500, China

Lan Qiu – School of Pharmacy, Chengdu Medical College, Chengdu, Sichuan Province 610500, China

Jin Liu – School of Pharmacy, Chengdu Medical College, Chengdu, Sichuan Province 610500, China

Renhan Dong – Chengdu Biobel Biotechnology Co., Ltd., Chengdu, Sichuan Province 610094, China

Wei Zhan – Chengdu Biobel Biotechnology Co., Ltd., Chengdu, Sichuan Province 610094, China

Chuanjun Qin – Chengdu Biobel Biotechnology Co., Ltd., Chengdu, Sichuan Province 610094, China

Complete contact information is available at:

<https://pubs.acs.org/10.1021/acsomega.2c03408>

Author Contributions

§J.P., Y.Z., and X.H. contributed equally

Notes

The authors declare no competing financial interest.

■ ACKNOWLEDGMENTS

J.P. performed most of the experiments, analyzed the data, and wrote the manuscript. Y.S.Z. and X.J.H. performed most of the experiments. S.H. performed the cell viability assay. Q.L. and S.T.T. performed the cell cycle arrest assay and Western blot analysis. X.F.G. and J.L. performed the in vivo study. D.T. performed the tubulin polymerization assay in vitro. R.H.D., W.Z., and C.J.Q. performed the synthesis of the compounds. B.G. and T.Y. conceived and designed the studies and wrote the manuscript. This study was supported by the Sichuan Science and Technology Program (2021JDRC0037, 2021ZYD0074) and Disciplinary Construction Innovation Team Foundation of Chengdu Medical College (CMC-XK-2103) and Graduate Innovation Fund (YCX2021-09, YCX2021-13).

■ ABBREVIATIONS

SCLC, small-cell lung cancer; MTIs, microtubule inhibitors; TCL, thin-layer chromatography; DMF, *N,N,N'*-tetramethyluronium tetrafluoroborate; IC₅₀, half-maximal inhibitory concentration; TBTU, *O*-(benzotriazol-1-yl)-*N,N,N',N'*-tetramethyluronium tetrafluoroborate; THF, tetrahydrofuran; DIAD, diethyl azodicarboxylate; PTSA, *p*-toluenesulfonic; SD, standard deviation; SEM, standard error of the mean; V_{max} , maximal velocity; IV, intravenous injection; BID, twice a day; TGI, tumor growth inhibition; NOD/SCID, non-obese diabetic/severe-combined immunodeficient; HP- β -CD, hydroxypropyl β cyclodextrin; IOD, integrated optical density

■ REFERENCES

- (1) Yang, X.; Man, J.; Chen, H.; Zhang, T.; Yin, X.; He, Q.; Lu, M. Temporal trends of the lung cancer mortality attributable to smoking from 1990 to 2017: A global, regional and national analysis. *Lung Cancer* **2021**, *152*, 49–57.
- (2) Siegel, R. L.; Miller, K. D.; Fuchs, H. E.; Jemal, A. Cancer Statistics, 2021. *Ca-Cancer J. Clin.* **2021**, *71*, 7–33.
- (3) Casiraghi, M.; Sedda, G.; Del Signore, E.; Piperno, G.; Maisonneuve, P.; Petrella, F.; de Marinis, F.; Spaggiari, L. Surgery for small cell lung cancer: When and how. *Lung Cancer* **2021**, *152*, 71–77.
- (4) National Institute for Health and Care Excellence. *Treating Small-cell Lung Cancer*; National Institute for Health and Care Excellence, 2021.

- (5) Zhang, L.; Hang, Y.; Liu, M.; Li, N.; Cai, H. First-Line Durvalumab Plus Platinum-Etoposide Versus Platinum-Etoposide for Extensive-Stage Small-Cell Lung Cancer: A Cost-Effectiveness Analysis. *Front. Oncol.* **2020**, *10*, 602185.
- (6) von Pawel, J. The role of topotecan in treating small cell lung cancer: second-line treatment. *Lung Cancer* **2003**, *41*, S3–S8.
- (7) Saltos, A.; Shafique, M.; Chiappori, A. Update on the Biology, Management, and Treatment of Small Cell Lung Cancer (SCLC). *Front. Oncol.* **2020**, *10*, 1074.
- (8) Perez, E. A. Microtubule inhibitors: Differentiating tubulin-inhibiting agents based on mechanisms of action, clinical activity, and resistance. *Mol. Cancer Ther.* **2009**, *8*, 2086–2095.
- (9) Jordan, M. A.; Wilson, L. Microtubules as a target for anticancer drugs. *Nat. Rev. Cancer* **2004**, *4*, 253–265.
- (10) Fanale, D.; Bronte, G.; Passiglia, F.; Calò, V.; Castiglia, M.; Di Piazza, F.; Barraco, N.; Cangemi, A.; Catarella, M. T.; Insalaco, L.; et al. Stabilizing versus destabilizing the microtubules: a double-edge sword for an effective cancer treatment option? *Anal. Cell Pathol.* **2015**, *2015*, 1.
- (11) (a) Ettinger, D. S.; Finkelstein, D. M.; Sarma, R. P.; Johnson, D. H. Phase II study of paclitaxel in patients with extensive-disease small-cell lung cancer: an Eastern Cooperative Oncology Group study. *J. Clin. Oncol.* **1995**, *13*, 1430–1435. (b) von Pawel, J.; Schiller, J. H.; Shepherd, F. A.; Fields, S. Z.; Kleisbauer, J. P.; Chrysson, N. G.; Stewart, D. J.; Clark, P. I.; Palmer, M. C.; Depierre, A.; et al. Topotecan versus cyclophosphamide, doxorubicin, and vincristine for the treatment of recurrent small-cell lung cancer. *J. Clin. Oncol.* **1999**, *17*, 658. (c) Owonikoko, T. K.; Niu, H.; Nackaerts, K.; Csoszi, T.; Ostoros, G.; Mark, Z.; Baik, C.; Joy, A. A.; Chouaid, C.; Jaime, J. C.; et al. Randomized Phase II Study of Paclitaxel plus Alisertib versus Paclitaxel plus Placebo as Second-Line Therapy for SCLC: Primary and Correlative Biomarker Analyses. *J. Thorac. Oncol.* **2020**, *15*, 274–287.
- (12) Irby, R. B.; Yeatman, T. J. Role of Src expression and activation in human cancer. *Oncogene* **2000**, *19*, S636–S642.
- (13) (a) Roelle, S.; Grosse, R.; Buech, T.; Chubanov, V.; Gudermaun, T. Essential role of Pyk2 and Src kinase activation in neuropeptide-induced proliferation of small cell lung cancer cells. *Oncogene* **2008**, *27*, 1737–1748. (b) Mellström, K.; Bjelfman, C.; Hammerling, U.; Pålman, S. Expression of c-src in cultured human neuroblastoma and small-cell lung carcinoma cell lines correlates with neurocrine differentiation. *Mol. Cell. Biol.* **1987**, *7*, 4178–4184.
- (14) Rosen, N.; Bolen, J. B.; Schwartz, A. M.; Cohen, P.; DeSeau, V.; Israel, M. A. Analysis of pp60c-src protein kinase activity in human tumor cell lines and tissues. *J. Biol. Chem.* **1986**, *261*, 13754–13759.
- (15) (a) Molina, J. R.; Foster, N. R.; Reungwetwattana, T.; Nelson, G. D.; Grainger, A. V.; Steen, P. D.; Stella, P. J.; Marks, R.; Wright, J.; Adjei, A. A. A phase II trial of the Src-kinase inhibitor saracatinib after four cycles of chemotherapy for patients with extensive stage small cell lung cancer: NCCTG trial N-0621. *Lung Cancer* **2014**, *85*, 245–250. (b) Miller, A. A.; Pang, H.; Hodgson, L.; Ramnath, N.; Otterson, G. A.; Kelley, M. J.; Kratzke, R. A.; Vokes, E. E.; Cancer; Leukemia Group, B. A phase II study of dasatinib in patients with chemosensitive relapsed small cell lung cancer (Cancer and Leukemia Group B 30602). *J. Thorac. Oncol.* **2010**, *5*, 380–384.
- (16) Arnst, K. E.; Banerjee, S.; Chen, H.; Deng, S.; Hwang, D. J.; Li, W.; Miller, D. D. Current advances of tubulin inhibitors as dual acting small molecules for cancer therapy. *Med. Res. Rev.* **2019**, *39*, 1398–1426.
- (17) Kanthou, C.; Tozer, G. M. Microtubule depolymerizing vascular disrupting agents: novel therapeutic agents for oncology and other pathologies. *Int. J. Exp. Pathol.* **2009**, *90*, 284–294.
- (18) Smolinski, M. P.; Bu, Y.; Clements, J.; Gelman, I. H.; Hegab, T.; Cutler, D. L.; Fang, J. W. S.; Fetterly, G.; Kwan, R.; Barnett, A.; et al. Discovery of Novel Dual Mechanism of Action Src Signaling and Tubulin Polymerization Inhibitors (KX2-391 and KX2-361). *J. Med. Chem.* **2018**, *61*, 4704–4719.
- (19) Blauvelt, A.; Kempers, S.; Lain, E.; Schlesinger, T.; Tyring, S.; Forman, S.; Ablon, G.; Martin, G.; Wang, H.; Cutler, D. L.; et al. Phase 3 Trials of Tirbanibulin Ointment for Actinic Keratosis. *N. Engl. J. Med.* **2021**, *384*, 512–520.
- (20) (a) Anbalagan, M.; Ali, A.; Jones, R. K.; Marsden, C. G.; Sheng, M.; Carrier, L.; Bu, Y.; Hangauer, D.; Rowan, B. G. Peptidomimetic Src/pretubulin inhibitor KX-01 alone and in combination with paclitaxel suppresses growth, metastasis in human ER/PR/HER2-negative tumor xenografts. *Mol. Cancer Ther.* **2012**, *11*, 1936–1947. (b) Anbalagan, M.; Carrier, L.; Glodowski, S.; Hangauer, D.; Shan, B.; Rowan, B. G. KX-01, a novel Src kinase inhibitor directed toward the peptide substrate site, synergizes with tamoxifen in estrogen receptor α positive breast cancer. *Breast Cancer Res. Treat.* **2012**, *132*, 391–409. (c) Liu, T.; Hu, W.; Dalton, H. J.; Choi, H. J.; Huang, J.; Kang, Y.; Pradeep, S.; Miyake, T.; Song, J. H.; Wen, Y.; et al. Targeting SRC and tubulin in mucinous ovarian carcinoma. *Clin. Cancer Res.* **2013**, *19*, 6532–6543.
- (21) Wang, L.; Zheng, Y.; Li, D.; Yang, J.; Lei, L.; Yan, W.; Zheng, W.; Tang, M.; Shi, M.; Zhang, R.; et al. Design, Synthesis, and Bioactivity Evaluation of Dual-Target Inhibitors of Tubulin and Src Kinase Guided by Crystal Structure. *J. Med. Chem.* **2021**, *64*, 8127–8141.
- (22) (a) Sun, L.; Tran, N.; Tang, F.; App, H.; Hirth, P.; McMahon, G.; Tang, C. Synthesis and biological evaluations of 3-substituted indolin-2-ones: a novel class of tyrosine kinase inhibitors that exhibit selectivity toward particular receptor tyrosine kinases. *J. Med. Chem.* **1998**, *41*, 2588–2603. (b) Salado, I. G.; Zaldivar-Diez, J.; Sebastian-Perez, V.; Li, L.; Geiger, L.; Gonzalez, S.; Campillo, N. E.; Gil, C.; Morales, A. V.; Perez, D. I.; et al. Leucine rich repeat kinase 2 (LRRK2) inhibitors based on indolinone scaffold: Potential pro-neurogenic agents. *Eur. J. Med. Chem.* **2017**, *138*, 328–342.
- (23) Hiller, G.; Weber, K. Radioimmunoassay for tubulin: a quantitative comparison of the tubulin content of different established tissue culture cells and tissues. *Cell* **1978**, *14*, 795.
- (24) Xu, W.; Doshi, A.; Lei, M.; Eck, M. J.; Harrison, S. C. Crystal structures of c-Src reveal features of its autoinhibitory mechanism. *Mol. Cell* **1999**, *3*, 629–638.
- (25) Roskoski, R., Jr. Src protein-tyrosine kinase structure, mechanism, and small molecule inhibitors. *Pharmacol. Res.* **2015**, *94*, 9–25.
- (26) Seidal, T.; Edvardsson, H. Expression of c-kit (CD117) and Ki67 provides information about the possible cell of origin and clinical course of gastrointestinal stromal tumours. *Histopathology* **1999**, *34*, 416–424.
- (27) Bonne, D.; Heuséle, C.; Simon, C.; Pantaloni, D. 4',6-Diamidino-2-phenylindole, a fluorescent probe for tubulin and microtubules. *J. Biol. Chem.* **1985**, *260*, 2819–2825.